

Transport of drugs by the multidrug transporter AcrB involves an access and a deep binding pocket that are separated by a switch-loop

Thomas Eicher^{a,b,1}, Hi-jea Cha^{a,1}, Markus A. Seeger^{b,c,1}, Lorenz Brandstätter^{a,b}, Jasmin El-Delik^a, Jürgen A. Bohnert^d, Winfried V. Kern^d, François Verrey^b, Markus G. Grütter^c, Kay Diederichs^e, and Klaas M. Pos^{a,2}

^aInstitute of Biochemistry and Cluster of Excellence Frankfurt–Macromolecular Complexes, Goethe-University Frankfurt, D-60438 Frankfurt am Main, Germany; ^bInstitute of Physiology and Zurich Centre for Integrative Human Physiology and ^cDepartment of Biochemistry, University of Zurich, CH-8057 Zurich, Switzerland; ^dCenter for Infectious Diseases and Travel Medicine, Department of Medicine, University Hospital, Albert-Ludwigs University, D-79106 Freiburg, Germany; and ^eDepartment of Biology, University of Konstanz, D-78457 Konstanz, Germany

Edited by Shimon Schuldiner, Hebrew University of Jerusalem, Jerusalem, Israel, and accepted by the Editorial Board February 28, 2012 (received for review September 12, 2011)

AcrAB-TolC is the major efflux protein complex in *Escherichia coli* extruding a vast variety of antimicrobial agents from the cell. The inner membrane component AcrB is a homotrimer, and it has been postulated that the monomers cycle consecutively through three conformational stages designated loose (L), tight (T), and open (O) in a concerted fashion. Binding of drugs has been shown at a periplasmic deep binding pocket in the T conformation. The initial drug-binding step and transport toward this drug-binding site has been elusive thus far. Here we report high resolution structures (1.9–2.25 Å) of AcrB/designed ankyrin repeat protein (DARPin) complexes with bound minocycline or doxorubicin. In the AcrB/doxorubicin cocrystal structure, binding of three doxorubicin molecules is apparent, with one doxorubicin molecule bound in the deep binding pocket of the T monomer and two doxorubicin molecules in a stacked sandwich arrangement in an access pocket at the lateral periplasmic cleft of the L monomer. This access pocket is separated from the deep binding pocket apparent in the T monomer by a switch-loop. The localization and conformational flexibility of this loop seems to be important for large substrates, because a G616N AcrB variant deficient in macrolide transport exhibits an altered conformation within this loop region. Transport seems to be a stepwise process of initial drug uptake in the access pocket of the L monomer and subsequent accommodation of the drug in the deep binding pocket during the L to T transition to the internal deep binding pocket of the T monomer.

antibiotics | multidrug resistance | drug efflux | RND transporter

The three-component AcrA/AcrB/TolC multidrug resistance pump provides the Gram-negative *Escherichia coli* cell with the necessary means to protect itself against a wide range of noxious compounds (1). AcrB resides in the inner membrane and is the energy transducing and substrate specificity determinant of the entire three-component pump assembly (2, 3). AcrA is the adapter component that associates the inner membrane pump with the TolC outer membrane channel (4, 5). Importantly, all three components are necessary to obtain the multidrug resistance phenotype (3, 4).

The first de novo AcrB crystal structure was solved via X-ray crystallography at 3.5 Å resolution by Murakami et al. (6) in 2002 [Protein Data Bank (PDB) ID code 1IWG] and showed a ligand-free homotrimeric assembly (Fig. S1 A and B). Each monomer contains a 12 transmembrane helices (TMs)-containing transmembrane domain, with TM4 and TM10 harboring essential titratable residues (D407, D408, and K940) inside the topological core (7) (Fig. S1C).

Approximately half of the protein's 1,049 amino acids form two extensive periplasmic loops connecting TM1 with TM2 and TM7 with TM8 and extends 70 Å into the periplasm, comprising the TolC docking domain and a porter domain (Fig. S1 A and B).

The latter domain is divided in subdomains PN1, PN2, PC1, and PC2, which are coupled by sequential proximity (PN1-PN2, PC1-PC2) and by sharing β -strands to form common β -sheets (PN2-PC1, PC2-PN1) (Fig. S1D). Between the PC1 and PC2 subdomains a cleft is apparent, oriented approximately perpendicular to the membrane plane (Fig. S1 B and D). In the center of the trimer, the TolC docking domain exhibits a funnel-like structure narrowing to a central pore, defined by α -helices (designated pore helices) of the PN1 subdomains of each monomer. This pore has a small diameter and does not allow drugs to pass. Toward the membrane plane, the central pore leads to a central cavity and further to a 30- to 35-Å-wide, presumably lipid-filled transmembrane hole defined by the ring-like arrangement of the TMs of the trimer (Fig. S1). Three vestibules at the monomer interface located just above the membrane plane lead toward the central cavity (Fig. S1 A and B). The periplasmic boundaries of these vestibule areas were recently shown to be accessible for the AcrB substrate Bodipy FL N-(2-aminoethyl) maleimide (8). Moreover, the substrate specificity of the entire AcrAB-TolC efflux machinery was found to be localized in the AcrB periplasmic porter domain (2), whereas the AcrB transmembrane domain seems to be essential for proton translocation (7, 9) (Fig. S1).

In 2006, three groups independently published an asymmetric structure of AcrB grown in the monoclinic space group C2 (10–12) (PDB entries: 2DHH, 2DR6, 2DRD, and 2GIF, 2.8–2.9 Å), triclinic space group P1 (11) (2HRT, 3.0 Å), and an AcrB structure including bound designed ankyrin repeat proteins (DARPins) grown in orthorhombic space group P2₁2₁2₁ (2J8S, 2.5 Å) (12). Within the asymmetric AcrB trimer, each monomer has a different conformation denoted as loose (L), tight (T), and open (O) (access, binding, and extrusion, respectively) (10–12), with the L (or access) state closest to the conformation of the monomers in the symmetric structure (6). Two of the deposited asymmetric structures based on 3.1- and 3.3-Å data of AcrB/

Author contributions: T.E., H.C., M.A.S., J.A.B., W.V.K., K.D., and K.M.P. designed research; T.E., H.C., M.A.S., J.E.-D., K.D., and K.M.P. performed research; M.G.G. contributed new reagents/analytic tools; T.E., H.C., M.A.S., L.B., F.V., K.D., and K.M.P. analyzed data; and T.E., M.A.S., K.D., and K.M.P. wrote the paper.

The authors declare no conflict of interest.

This article is a PNAS Direct Submission. S.S. is a guest editor invited by the Editorial Board.

Data deposition: The atomic coordinates and structure factors reported in this paper have been deposited in the Protein Data Bank, www.pdb.org [PDB ID codes 4DX5 (WT AcrB/DARPin in complex with minocycline), 4DX6 (AcrB_G616N), and 4DX7 (WT AcrB/DARPin in complex with doxorubicin)].

¹T.E., H.C., and M.A.S. contributed equally to this work.

²To whom correspondence should be addressed. E-mail: pos@em.uni-frankfurt.de.

This article contains supporting information online at www.pnas.org/lookup/suppl/doi:10.1073/pnas.1114944109/-DCSupplemental.

minocycline and AcrB/doxorubicin cocrystals, respectively (10), showed binding of (9-bromo) minocycline or doxorubicin to a hydrophobic binding pocket exclusively present in one of the monomers (the T or binding monomer) within the asymmetric AcrB trimer. The DARPin bound AcrB structure was almost identical to the AcrB structures crystallized without binder, with rmsd of the superimposed trimeric structures ≤ 1 Å. The DARPin molecules only bind to the L and T conformers, resulting in a ratio of two DARPin molecules per AcrB trimer. This stoichiometry was verified by densitometry after microchannel electrophoresis, sedimentation velocity experiments, and via laser-induced liquid bead ion desorption mass spectrometry, suggesting that in solution and probably also in vivo AcrB adopts mainly the asymmetric conformation (12, 13).

In analogy with the functional rotation of the α/β -subunits of the F_1F_0 ATPase leading to synthesis of ATP (14), a similar catalytic mechanism was postulated for AcrB leading to drug export (10–12). In short, the hypothesis states that within the asymmetric trimer, the monomers can adopt any of the conformational states L, T, and O. Transport depends on the concerted—but not necessarily synchronous—cycling of the monomers through the states L, T, O, and back to L, which is the essence of the functional rotation. In the L conformation, substrates are recruited from the periplasmic space and/or the membrane for transport during the L to T transition toward the deep substrate binding pocket inside the porter domain. Upon conformational change toward the O state, substrate is released from the binding pocket and exits AcrB via its central funnel toward the TolC tunnel. During a complete functional rotation, occlusions and constrictions inside the porter domain seem to propagate from a lateral opening toward the central funnel driving the unidirectional transport of substrate. Hence, this mechanism was dubbed “peristaltic pump mechanism” (11, 15, 16) (Fig. S1 E–G). The conversion from T to O is suggested to be the energy-requiring step, in analogy to the binding change mechanism for the F_1F_0 ATPase (14). Drug efflux is also subject of bi-site activation; that is, the T to O transition within the LTO trimer (and the resulting release of the drug) only occurs when additional substrate has bound to the adjacent monomer. Strengthening this view are the recently observed strong cooperative kinetics of the extrusion of β -lactam antibiotics by the AcrAB-TolC system (17, 18).

The functional rotation mechanism suggests interdependence of the monomers, which means that inactivation of only one of the monomers will render the entire trimer inactive. Recently, this has been impressively shown to be the case by Nikaido and coworkers by the use of a covalently linked AcrB trimer (19). The proposed conformational cycling and the substantial rearrangement of the periplasmic subdomains was analyzed in vivo by the introduction of cysteine pairs (20, 21), whereby formation of disulfide bonds significantly decreased AcrB-mediated transport and restoring activity by the addition of the reducing reagent DTT.

Two conformationally distinct trimeric AcrB structures are known to date: the symmetric LLL (all loose) conformation (6) and the asymmetric LTO conformation (10–12). The very recently published crystal structure of the Cu^+ and Ag^+ transporter CusA from *E. coli* showed substrates bound to the periplasmic porter domain in all three protomers adapting a symmetric conformation with structural features describing a TTT conformation (22).

Most of the published AcrB structures are in the symmetric conformation but show in particular cases slight deviations between each other, indicating intrinsic flexibility (6, 7, 23–26). The LLL conformation has been postulated the “resting state”—in the absence of substrate (7, 15)—with the structural flexibility necessary for substrate acquisition (25). Recently published symmetric LLL state structures (at 3.85- to 3.2-Å resolution) were shown to accommodate substrates to the inner wall of the transmembrane cavity (25–27) or in the open cleft determined by

the PC1/PC2 subdomains, constituting the access to tunnel 2 (Fig. S1 E and F) (24, 27). One transport hypothesis assumes the substrate to be garnered from the outer leaflet of the inner membrane or directly from the periplasm. Substrates that are partitioned in the outer leaflet of the inner membrane might enter the L monomer via the TM8/TM9 groove, whereas substrates located in the periplasm might enter the L monomer via the PC1/PC2 cleft (i.e., the entrance of tunnel 2 ≈ 15 Å above the membrane plane) (Fig. S1 E). Additionally, a concerted and consecutive drug uptake via the TM8/TM9 groove and subsequent transport to the PC1/PC2 cleft might be envisioned.

High-resolution (2.5 Å) data describing the asymmetric trimer show clear densities in the TM8/TM9 groove of the L monomer, which has been attributed to the highly concentrated detergent and AcrB substrate *n*-dodecyl- β -D-maltoside (12). Upon conformational change from the L to the T state, tunnel 1 appears and might provide one of the pathways for substrates toward the hydrophobic deep binding pocket that accommodates the substrate molecule.

Upon transition from the T to the O state, the binding pocket closes again; substrate is squeezed out and follows a newly formed tunnel (tunnel 3) to the funnel, and is from there finally extruded into the medium via TolC (Fig. S1).

In the work presented here, high-resolution structures (1.9 and 2.25 Å) describe a potential initial binding step of doxorubicin in the L conformer, and multiple substrate (minocycline or doxorubicin and dodecyl- α -D-maltoside) binding to the T conformer. Access to the internal deep binding pocket in the T monomer is mediated by the conformational change from the L to the T conformation. In the L monomer, two doxorubicin molecules are positioned in an access pocket and separated from the internal binding pocket by a flexible loop, designated switch-loop, containing F615 and F617. The observations lead to the hypothesis of a stepwise transport of drugs initially bound to the access pocket in the L conformation and subsequent transport to the deep binding pocket by the conformational change of the switch-loop and the PN2/PC1 subdomains during the L to T transition.

Results

Binding of Minocycline and Doxorubicin by the AcrB Wild-Type Protein. We describe here the crystallization and structural elucidation of AcrB/DARPin complexes in the presence of minocycline and doxorubicin based on 1.9-Å and 2.25-Å diffraction data (Table S1). AcrB/DARPin complexes were cocrystallized in the presence of minocycline (2.0 mM) or doxorubicin (0.4 mM), yielding orthorhombic crystals. The structures were refined to an R_{free} of 23.1% and 22.7%, respectively, and describe an asymmetric trimer comprising three different monomer conformations representing the consecutive states L, T, and O (15). Electron densities for minocycline or doxorubicin could be clearly identified in the hydrophobic deep binding pocket of the T monomer (Fig. 1 and Fig. S2). Whereas the position of minocycline is congruent with the structure of Murakami et al. (10), the orientation of the doxorubicin molecule inside the deep binding pocket differs substantially (Fig. S2 and Table S2). Notably, differences in crystallization conditions and resolution, and our use of crystallization chaperones (DARPins), are possible reasons for the observed distinctions. In the T monomer, another density located in the lateral cleft determined by the PC1 and PC2 subdomains of the periplasmic porter domain could be assigned to dodecyl- α -D-maltoside (Fig. S3). In the L monomer of the AcrB/doxorubicin cocrystal structure, but not in the AcrB/minocycline cocrystal structure, large densities were observed at the PC1/PC2 subdomain cleft (access pocket) and could be assigned to a twofold symmetric sandwich of stacked doxorubicin molecules (Fig. 2 and Fig. S4). The AcrB/doxorubicin cocrystal structure therefore reveals an asymmetric AcrB trimer containing three doxorubicin molecules: two doxorubicin molecules

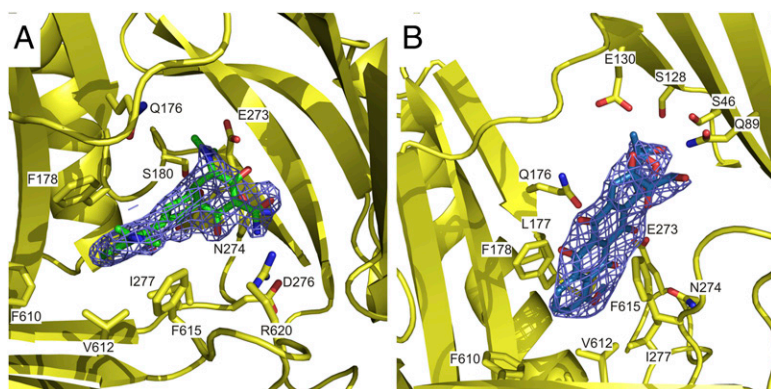


Fig. 1. Binding of minocycline (A) and doxorubicin (B) in the deep binding pocket of the T monomer of the AcrB trimer. Binding of the substrate molecules is mainly achieved by aromatic stacking interactions and polar interactions by the indicated side chains. The mesh represents the $2F_o - F_c$ electron density map contoured at 1.1σ . (A) AcrB/minocycline complex. The dimethylamino moiety of the drug is sandwiched between F178 and F615. The carboxamid group interacts with the polar side chain of N274. (B) AcrB/doxorubicin complex. F178 and F615 wedge the C and D rings of doxorubicin. At the other end of the molecule, Q89 interacts with the hydroxyl group of the dihydroxypropanone moiety and also, together with side chain S46, S128, and E130, with the daunosamine sugar moiety.

bound to the access pocket in the L monomer and one bound to the deep binding pocket in the T monomer (Fig. S5). This observation indicates a possible link between the initial binding of drugs in the L monomer and the subsequent binding of the drug in the deep binding pocket mediated by the L to T transition in the functional rotation cycle (Figs. S1 E–G and S5).

Coordination of doxorubicin by residues inside the AcrB access pocket includes hydrophobic interactions with F666 and L828 and charged/polar interactions with T676, R717, and N719 (Fig. S4). In a recent study, these coordination sites and further proximate residues (D566, F664, L668, and E673; Fig. S4) were Cys-substituted and accessible to the AcrB substrate Bodipy FL maleimide (28), matching the crystallographic data presented here (Fig. S4B). Furthermore, single alanine substitution of residues F664, F666, E673, and R717 markedly interfered with the ability of these AcrB variants to confer resistance toward various toxic compounds (27).

The L monomer is considered the access protomer (10, 11) involved in the initial stage of drug binding. The lateral access pocket at the periplasmic cleft confined by the PC1 and PC2 subdomains might be the initial entry point for drugs to the AcrB functional rotation cycle. However, many of the AcrB substrates are expected also to partition into the outer leaflet of the inner membrane because of their hydrophobic properties. A suggested entry pathway for drugs partitioned in the outer leaflet of the inner membrane is the hydrophobic groove in the transmembrane domain defined by TM8 and TM9 (6, 15), where in the high-resolution structures presented here, binding of the detergent and AcrB substrate dodecyl- β -D-maltoside is apparent (Fig. S6 A and B).

The TM8/TM9 groove defines the entrance to tunnel 1 (Fig. S1F) (12, 15) inside the periplasmic porter domain, which leads toward the hydrophobic deep binding pocket (10–12). This tunnel and the opening of the deep binding pocket with subsequent minocycline or doxorubicin binding are apparent after the L to T transition (Fig. 1 and ref. 10). The L monomer of the AcrB/doxorubicin structure comprises one dodecyl- β -D-maltoside molecule at the TM8/TM9 transmembrane groove and a doxorubicin dimer sandwich at the access pocket (Figs. S4 and S6). The access pocket and the TM8/TM9 groove might represent exclusive entry points for drugs with different properties, or consecutive gates in a multistep transport mechanism.

A Switch-Loop Separates Access and Deep Binding Pocket Areas. The doxorubicin molecules in the access pocket of the L monomer

are separated from the deep binding pocket (Fig. 1) by a loop containing F615, F617, and R620 (switch-loop; Fig. 2 A and B).

The switch-loop adopts alternative conformations in the L and T monomer. It seems to modulate the path from the access pocket in the L conformation to the deep binding pocket in the T conformation. Superimposition of the L and T conformations indicates that the side chain conformation of F615 (located on the switch-loop) and Q176 (located on the PN2 subdomain) seen in the L monomer would interfere with doxorubicin binding in the deep binding pocket, and the switch-loop main chain conformation in the T conformation would sterically interfere with the stacked doxorubicin location as observed in the L conformation. Therefore, steric hindrance presumably precludes binding of the drugs in the deep binding pocket in the L monomer, whereas the alternative loop conformation seems to prevent binding of doxorubicin to the access pocket in the T conformation (Fig. 2B). The switch-loop conformation in the structure of the symmetric AcrB (i.e., the LLL conformation) is less inward oriented and would theoretically interfere with doxorubicin binding if these would localize at the same position as observed in the asymmetric LTO AcrB trimer (Fig. S7). Substrates like ethidium (PDB ID code: 1T9X, 3.1 Å) (27) or taurocholate (PDB ID code: 2W1B, 3.85 Å) (24) seem to bind more at the periphery of the PC1/PC2 cleft compared with doxorubicin binding in the asymmetric cocrystal structure (Fig. S7C).

It was recently reported (29) that a single substitution in the switch loop (G616N) decreases AcrB's ability to extrude macrolides, resembling the poor efflux activity toward macrolides shown by the *Pseudomonas aeruginosa* homolog MexB (wild-type MexB contains N616). The switch-loop conformation in the L conformation of the AcrB G616N variant (solved at 2.9 Å in the presence of minocycline; Table S1) resembles the loop conformation of wild-type AcrB in the T monomer and of the switch-loop conformation found in the wild-type MexB L monomer structure (Fig. 2 B and C). The differences in the switch-loop conformations between the wild-type AcrB and G616N variant are clearly defined by the differences in electron density in this region of the protein (Fig. S6 C and D).

Superimposition of the L monomer structure of MexB or AcrB G616N variant on the AcrB wild-type L monomer structure predicts a minor steric clash with one of the doxorubicin molecules bound the access pocket of wild-type AcrB (Fig. 2C). We conducted a drug resistance assay on solid medium using *E. coli* BW25113 Δ acrB comprising wild-type or G616N AcrB equally well expressed from plasmids (Fig. S8). Clearly, an effect

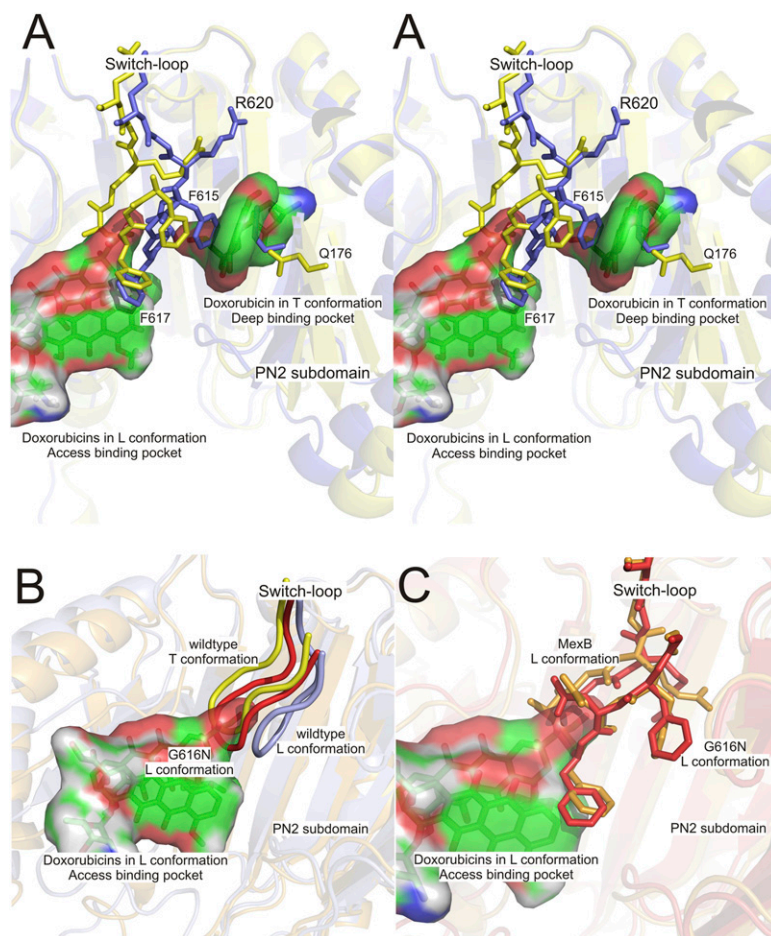


Fig. 2. Switch-loop conformations of wild-type AcrB, G616N variant, and MexB. (A) Cross-eyed stereo representation of the superimposition of the access pocket of the L monomer (blue) and deep binding pocket of the T monomer (yellow). The doxorubicin dimer sandwich is shown in stick and surface representation accommodated in the access pocket on the left. Doxorubicin located in the deep binding pocket in the T monomer (stick and surface representation) is flanked by the PN2 and PC1 subdomains (PC1 subdomain not shown for clarity). The switch-loop (including residues F615, F617, and R620 depicted here) adopts different conformations in the L monomer (blue) and T monomer (yellow). The backbone orientation of the switch-loop in the T conformation (yellow) coincides with the doxorubicin dimer sandwich location. Residues Q176 and F615 in the L conformation (blue) are representative for the steric hindrance (caused by the switch-loop and PN2 subdomain, respectively) preventing doxorubicin binding in the deep binding pocket. (B) Superimposition of the wild-type AcrB and G616N variant at the access binding pocket region. At left is the doxorubicin dimer sandwich (in stick and surface representation) accommodated in the wild-type AcrB L conformation access pocket and the switch-loops of the different conformations in AcrB wild-type (L conformation, blue; T conformation, yellow) and G616N variant (L conformation, red). The switch-loop of the G616N variant in the L conformation adopts a conformation commensurable with the switch-loop conformation in the AcrB wild-type T conformation. (C) At left is the doxorubicin dimer sandwich (in stick and surface representation) accommodated in the wild-type AcrB L conformation access pocket and the switch-loops of the G616N variant (red) and MexB (PDB ID code 2V50, orange) in the L conformation. Both switch-loops of the G616N variant and MexB are in the L conformation and adopt a conformation commensurable with the switch-loop conformation in the AcrB wild-type T conformation (see B). MexB and G616N both have substantially lower macrolide efflux activity (29).

of the G616N substitution on the resistance against erythromycin could be detected, and a subtle difference in growth in the presence of doxorubicin was observed. Growth on other substrates like novobiocin, ethidium, or chloramphenicol was, however, also slightly affected by the substitution in various degrees. In minimal inhibitory concentration (MIC) experiments reported recently (29) using liquid media and chromosomal substitution of the G616N variant in an *E. coli* AG100 background, larger macrolide molecules were substantially less well transported by this variant, whereas other substrates like novobiocin, ethidium, and chloramphenicol showed wild-type resistance. Specific sensitivity toward macrolides was also conferred when F615 (localized on the switch-loop) was substituted with Ala, or when residues 615–617 were deleted from the loop (30).

Discussion

Access, Binding, and Extrusion, the Three Cyclic actions Mediated by the L, T, and O Monomer. The structural information obtained in this study from crystallization and structural elucidation of the wild-type AcrB with bound minocycline and doxorubicin at unprecedented high resolution, as well as the structures of the AcrB variant G616N, can be combined in a model for access, binding, and extrusion of drugs catalyzed by AcrB. Homotrimeric AcrB can adopt three different monomer conformations representing the consecutive states L, T, and O. However, during transition of the conformations within the trimer, AcrB is anticipated to exist in intermediate states [e.g., TTO (15, 16)], a hypothesis that is supported by quantitative cysteine cross-link experiments and molecular dynamics studies (21, 31).

The LTO conformation most likely represents the lowest energy form of the AcrB trimer in the presence of substrate (15, 16, 31), given that in vivo cross-link studies (21) and analytical ultracentrifugation experiments in the presence of DARPins (12, 13) imply the presence of this conformation in the membrane and in detergent rather than the readily crystallizable LLL form. The latter state might preferably exist in the absence of ligands (i.e., “resting state”), as has been suggested previously (7, 15, 31), and apparently is preferred within the R32 crystal lattice. Once substrates are present in the periplasmic space and/or partitioned in the periplasmic space/inner-membrane boundary, AcrB-catalyzed efflux of the drugs over the outer membrane is counteracting the influx. The L monomer provides probable initial binding sites for drugs to enter the AcrB protein. One entry point might be the TM8/TM9 groove located at the height of the periplasm/membrane boundary (i.e., the outer leaflet of the inner membrane). In the high-resolution structures presented here (Fig. S6) and in the 2.5-Å structure by Sennhauser et al. (12), a dodecyl- β -D-maltoside molecule is deeply buried inside the TM8/TM9 transmembrane groove, unlike the other more loosely bound dodecyl- β -D-maltoside molecules that were assigned from the data of the electron density maps. Moreover, this groove is located exactly below tunnel 2 (Fig. S1F) in the T monomer leading to the deep binding pocket (12, 15). In addition, recent Bodipy FL *N*-(2-aminoethyl) maleimide labeling data indicated that residue S836, located at the entrance of tunnel 2 on the PC2 subdomain, was highly accessible for this AcrB substrate (8). A second entry point is postulated at a lateral access pocket at the periplasmic cleft confined by the PC1 and PC2 subdomains (Fig. 2 and Figs. S1B and D, S4, and S7). Both putative entry sites might represent exclusive access points for drugs with different

properties, or consecutive binding sites. Interestingly, both sites collapse during the proton motive force dependent T to O transition simultaneous with the closure of the deep binding pocket and the disappearance of the tunnels leading from both these putative drug entry points toward the deep binding pocket (11, 12, 15).

The postulated entry step at the periplasmic cleft is depicted by the doxorubicin sandwich inside the access pocket of the L monomer (Fig. 3A). Binding of substrates (ethidium, rhodamine 6G, ciprofloxacin, nafcillin, Phe-Arg- β -naphthylamide, and taurocholate) was also shown in the symmetric L-state trimer (24, 27) at a more lateral position of the PC1/PC2 cleft (Fig. S7). The more lateral binding might indicate an earlier step in substrate acquisition by the complete ligand-free “resting-state” LLL trimer or might indicate the promiscuity of binding different

drugs to different sites within the cleft area. Although it is unclear why two doxorubicin molecules are bound to the L monomer of the asymmetric trimer, it seems that one of the drug molecules can be further transported deeper into the AcrB protein toward the T monomer deep binding pocket (Fig. 3B). Very recently, cocrystal structures from 3.3-Å X-ray data showed the binding of high-molecular-mass drugs erythromycin and rifampicin to the access pocket, whereas the low-molecular-mass substrates like minocyclin and doxorubicin were postulated to be transported directly to the deep binding pocket, without binding first to the access pocket (32). Because doxorubicin is mainly present as dimer in solution at concentrations at which the AcrAB-TolC efflux system confers resistance to *E. coli* against the drug (and at the concentrations used for cocrystallization) (33), the binding in a dimeric state in the access pocket might represent a preliminary stage to the binding of the doxorubicin monomer in the deep binding pocket. This entails prerequisite conformational flexibility between the L and T monomer, as well as a binding affinity difference of the access pocket (low affinity) and deep binding pocket (high affinity). The switch-loop and the β -sheets of the PN2/PC1 subdomains prohibit entry of the drug in the deep binding pocket in the L conformation (Fig. 2), and rearrangement of these structures in the L to T transition facilitates access to the deep binding pocket in the T monomer (Fig. 3B). The presence of dodecyl- α -D-maltoside in the PC1/PC2 cleft of the T monomer seems to contradict the predicted function of the switch-loop. The maltoside moiety of dodecyl- α -D-maltoside is localized at the same position as the daunosamine sugar ring of one of the doxorubicin molecules in the L monomer, whereas the aliphatic tail protrudes into the porter domain and seems not to interfere with the switch loop conformation in the T monomer (Fig. S3). The presence of dodecyl- α -D-maltoside at this position in the T monomer is puzzling, even more so given that the high resolution of the electron density maps did allow to clearly distinguish between the α - and β -anomers of this detergent. Because only low concentrations of α -anomer are present in the commercial batch of dodecyl- β -D-maltoside, the binding must occur with high affinity for this ligand.

Once binding of drug to the deep binding pocket occurs, it is most likely stabilizing the T conformation and is enabling further stabilization by the PN1 subdomain tilting of the neighboring monomer (Fig. 3B). Thus, submovement of the subdomains PN2/PC1 in the L to T transition not only takes effect on further conformational changes in the same monomer (i.e., T to O transition) (Fig. 3C) but is also implied to have an effect on the conformational changes in the neighboring monomers.

Movement of the subdomains during the T to O transition is coupled to an extensive kinking of TM8, which seems to be coupled to conformational changes in the transmembrane domain. Most likely protonation events [i.e., uptake of protons from the periplasm to the proton relay residues (D407/D408) located in the transmembrane domain] lead to a conformational change of the TMs, and this movement is presumably transduced to TM8, which is connected to the PN1/PC2 subdomains. Once the drug has been released from the O conformation, a switch to the L conformation to initiate another round of drug binding in the access pocket seems necessary (Fig. 3D). The reorientation of the PN1/PC2 subdomains during the O to L transition leads to de-kinking of TM8, which possibly triggers the deprotonation events in the transmembrane domain, stabilizing the L monomer conformation, and a new round of antibiotic uptake via the TM8/TM9 groove and/or access pocket can be started (Fig. 3). Molecular insight into coupling of the protonation and deprotonation events in the transmembrane domain to the conformational changes in the periplasmic porter domain leading to drug efflux will eventually provide the complete chain of events of proton motive force-driven drug extrusion by AcrB.

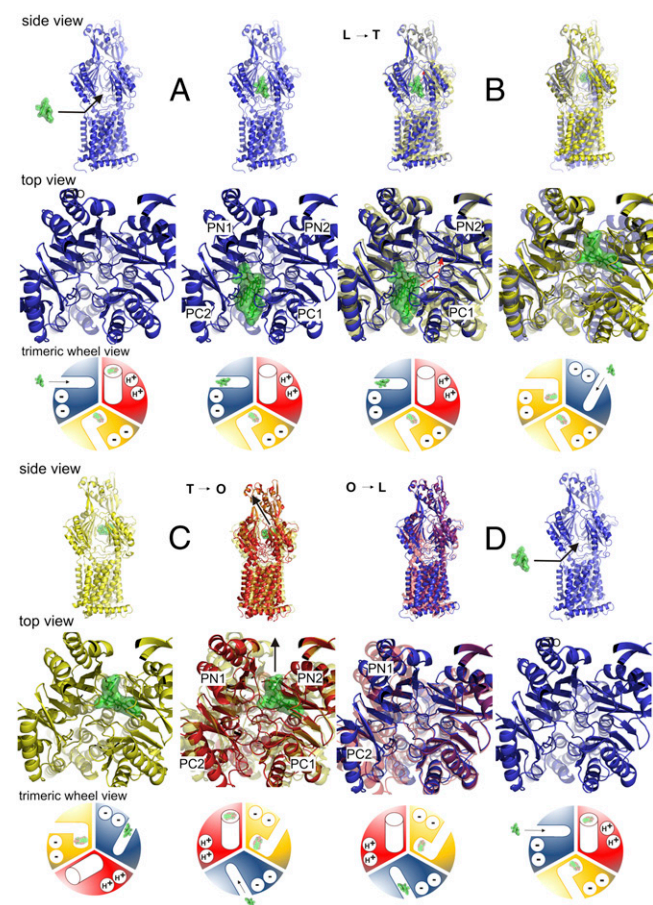


Fig. 3. Stepwise AcrB-catalyzed drug transport mediated by cyclic conformations L (blue), T (yellow), and O (red). (A–D) Sequential drug transport steps and conformational cycling of one AcrB monomer within the trimer. *Top:* Side view of the monomer parallel to the membrane plane; the view is toward the PC1 and PC2 subdomains and the access pocket region. *Middle:* View on the porter domain perpendicular to the membrane plane. *Bottom:* Trimeric wheel view displays the state of the monomer from *Top* and *Middle* (upper left monomer in the wheel, L in blue, T in yellow, and O in red) in A–D in relation to the other monomers in the AcrB trimer. Substrate (doxorubicin) is depicted in green. The putative protonation state of D407 and D408 inside the transmembrane domain is indicated (L and T are deprotonated, O is protonated). (A) Initial drug uptake via the access pocket in the L monomer. (B) Transfer of the drug from the low-affinity access pocket to the high-affinity deep binding pocket during the L to T transition. (C) Directional drug transport during the T to O transition. Subdomains PC1 and PC2 close the lateral access and prevent backsliding of the drug, which is extruded through tunnel 3. (D) Resetting the monomer by the O to L transition to reinitialize drug uptake via the access pocket.

Materials and Methods

Bacterial Strains, Plasmids, and Growth Conditions. *E. coli* DH5 α was used as host for cloning procedures. *E. coli* C43 (DE3) (34) harboring pET24acrB_{His} (35) and pET24acrB_{His}_G616N was used for protein overproduction. LB medium and LB agar (36) were used for routine bacterial growth at 37 °C. Kanamycin (Applichem) was used at 50 $\mu\text{g mL}^{-1}$ (Kan⁵⁰). Drug resistance was assayed using solid media, as described previously (37).

Site-Directed Mutagenesis. pET24acrB_{His} (35) served as a template for site-directed mutagenesis. By using the Quikchange protocol (Stratagene), amino acid substitution was achieved with 5' phosphorylated primers. Insertion of mutation was verified by sequencing (Microsynth).

Crystallization of AcrB Wild Type and G616N in Presence of DARPins. Overexpression and purification of DARPIn clone 1108_19 was accomplished as previously described (12). AcrB wild-type and AcrB_G616N were overproduced according to the method reported previously (11, 35), with the following variations for G616N. Expression was induced with IPTG (1 mM) at OD₆₀₀ = 0.8, and the culture was incubated overnight at 20 °C, producing up to 20 mg AcrB_G616N per liter of culture after affinity chromatography. Because of the tendency of AcrB_G616N to aggregate, the protein concentration for crystallization was experimentally determined to be optimal at 8 mg mL⁻¹. DARPins synthesis, purification, and AcrB/DARPIn complex crystallization were done according to Sennhauser et al. (12) using *n*-dodecyl- β -D-maltoside (Glycon; with 0.01% α -isomer). Substrate was added before crystallization at concentrations of 2 mM and 0.4 mM for minocycline or doxorubicin, respectively. Crystals (AcrB/DARPIn and G616N/

DARPIn complex) were grown by the hanging drop vapor diffusion method at 0.05 M *N*-(2-Acetamido)-iminodiacetic acid buffer (pH 6.5), 7–9% (wt/vol) polyethylene glycol (PEG) 4000, 6–10% (vol/vol) glycerol, and 0.2 M (NH₄)₂SO₄. AcrB_G616N/DARPIn crystals were grown in the presence of minocycline (2 mM final concentration), but electron densities at 2.9 Å at the expected deep binding pocket location were too weak to assign minocycline binding at this position.

X-Ray Diffraction Dataset Analysis and Refinement Procedure. Datasets of P2₁2₁ crystals were collected at the beamline X06SA of the Swiss Light Source (Paul Scherrer Institut) (wavelength 0.8–1.0 Å). Data reduction was done with the XDS package (38). The structures were solved by molecular replacement using MOLREP (39) or PHASER (40). Refinement was performed with the program phenix.refine from the PHENIX package (41) using rigid body refinement followed by restrained refinement with translation libration screw (TLS) restraints. Model rebuilding was performed using the program COOT (42). For superimposition of the AcrB monomers and ligands, the program SUPERPOSE (43) was used matching the DN (residues 181–272) and DC (residues 724–812) subdomains (11). Figures were created using Pymol (www.pymol.org).

ACKNOWLEDGMENTS. We thank the beamline staff at the protein crystallography X06SA beamline (Swiss Light Source, SLS) of the Paul Scherrer Institute (Villigen, Switzerland). This work was supported by the Swiss National Foundation, the German Research Foundation (SFB 807, Transport and Communication across Biological Membranes) (K.M.P.), the Swiss National Center of Competence in Research (NCCR) Structural Biology, and the Forschungskredit der Universität Zürich (L.B.). K.M.P. is supported by the DFG-EXC115 (Cluster of Excellence Macromolecular Complexes at the Goethe-University Frankfurt).

- Nikaido H, Takatsuka Y (2009) Mechanisms of RND multidrug efflux pumps. *Biochim Biophys Acta* 1794:769–781.
- Elkins CA, Nikaido H (2002) Substrate specificity of the RND-type multidrug efflux pumps AcrB and AcrD of *Escherichia coli* is determined predominantly by two large periplasmic loops. *J Bacteriol* 184:6490–6498.
- Ma D, et al. (1995) Genes *acrA* and *acrB* encode a stress-induced efflux system of *Escherichia coli*. *Mol Microbiol* 16:45–55.
- Fralick JA (1996) Evidence that TolC is required for functioning of the Mar/AcrAB efflux pump of *Escherichia coli*. *J Bacteriol* 178:5803–5805.
- Symmons MF, Bokma E, Koronakis E, Hughes C, Koronakis V (2009) The assembled structure of a complete tripartite bacterial multidrug efflux pump. *Proc Natl Acad Sci USA* 106:7173–7178.
- Murakami S, Nakashima R, Yamashita E, Yamaguchi A (2002) Crystal structure of bacterial multidrug efflux transporter AcrB. *Nature* 419:587–593.
- Su CC, et al. (2006) Conformation of the AcrB multidrug efflux pump in mutants of the putative proton relay pathway. *J Bacteriol* 188:7290–7296.
- Husain F, Bikhchandani M, Nikaido H (2011) Vestibules are part of the substrate path in the multidrug efflux transporter AcrB of *Escherichia coli*. *J Bacteriol* 193:5847–5849.
- Seeger MA, von Ballmoos C, Verrey F, Pos KM (2009) Crucial role of Asp408 in the proton translocation pathway of multidrug transporter AcrB: Evidence from site-directed mutagenesis and carbodiimide labeling. *Biochemistry* 48:5801–5812.
- Murakami S, Nakashima R, Yamashita E, Matsumoto T, Yamaguchi A (2006) Crystal structures of a multidrug transporter reveal a functionally rotating mechanism. *Nature* 443:173–179.
- Seeger MA, et al. (2006) Structural asymmetry of AcrB trimer suggests a peristaltic pump mechanism. *Science* 313:1295–1298.
- Sennhauser G, Amstutz P, Briand C, Storchenegger O, Grütter MG (2007) Drug export pathway of multidrug exporter AcrB revealed by DARPIn inhibitors. *PLoS Biol* 5:e7.
- Brandstätter L, et al. (2011) Analysis of AcrB and AcrB/DARPIn ligand complexes by LILBID MS. *Biochim Biophys Acta* 1808:2189–2196.
- Boyer PD (1997) The ATP synthase—a splendid molecular machine. *Annu Rev Biochem* 66:717–749.
- Pos KM (2009) Drug transport mechanism of the AcrB efflux pump. *Biochim Biophys Acta* 1794:782–793.
- Seeger MA, et al. (2008) The AcrB efflux pump: Conformational cycling and peristalsis lead to multidrug resistance. *Curr Drug Targets* 9:729–749.
- Lim SP, Nikaido H (2010) Kinetic parameters of efflux of penicillins by the multidrug efflux transporter AcrAB-TolC of *Escherichia coli*. *Antimicrob Agents Chemother* 54:1800–1806.
- Nagano K, Nikaido H (2009) Kinetic behavior of the major multidrug efflux pump AcrB of *Escherichia coli*. *Proc Natl Acad Sci USA* 106:5854–5858.
- Takatsuka Y, Nikaido H (2009) Covalently linked trimer of the AcrB multidrug efflux pump provides support for the functional rotating mechanism. *J Bacteriol* 191:1729–1737.
- Takatsuka Y, Nikaido H (2007) Site-directed disulfide cross-linking shows that cleft flexibility in the periplasmic domain is needed for the multidrug efflux pump AcrB of *Escherichia coli*. *J Bacteriol* 189:8677–8684.
- Seeger MA, et al. (2008) Engineered disulfide bonds support the functional rotation mechanism of multidrug efflux pump AcrB. *Nat Struct Mol Biol* 15:199–205.
- Long F, et al. (2010) Crystal structures of the CusA efflux pump suggest methionine-mediated metal transport. *Nature* 467:484–488.
- Das D, et al. (2007) Crystal structure of the multidrug efflux transporter AcrB at 3.1 Å resolution reveals the N-terminal region with conserved amino acids. *J Struct Biol* 158:494–502.
- Drew D, et al. (2008) The structure of the efflux pump AcrB in complex with bile acid. *Mol Membr Biol* 25:677–682.
- Törnroth-Horsefield S, et al. (2007) Crystal structure of AcrB in complex with a single transmembrane subunit reveals another twist. *Structure* 15:1663–1673.
- Yu EW, McDermott G, Zgurskaya HI, Nikaido H, Koshland DE, Jr. (2003) Structural basis of multiple drug-binding capacity of the AcrB multidrug efflux pump. *Science* 300:976–980.
- Yu EW, Aires JR, McDermott G, Nikaido H (2005) A periplasmic drug-binding site of the AcrB multidrug efflux pump: A crystallographic and site-directed mutagenesis study. *J Bacteriol* 187:6804–6815.
- Husain F, Nikaido H (2010) Substrate path in the AcrB multidrug efflux pump of *Escherichia coli*. *Mol Microbiol* 78:320–330.
- Wehmeier C, Schuster S, Fährnich E, Kern WV, Bohnert JA (2009) Site-directed mutagenesis reveals amino acid residues in the *Escherichia coli* RND efflux pump AcrB that confer macrolide resistance. *Antimicrob Agents Chemother* 53:329–330.
- Bohnert JA, et al. (2008) Site-directed mutagenesis reveals putative substrate binding residues in the *Escherichia coli* RND efflux pump AcrB. *J Bacteriol* 190:8225–8229.
- Yao XQ, Kenzaki H, Murakami S, Takada S (2010) Drug export and allosteric coupling in a multidrug transporter revealed by molecular simulations. *Nat Commun* 1:117.
- Nakashima R, Sakurai K, Yamasaki S, Nishino K, Yamaguchi A (2011) Structures of the multidrug exporter AcrB reveal a proximal multisite drug-binding pocket. *Nature* 480:565–569.
- Menozzi M, Valentini L, Vannini E, Arcamone F (1984) Self-association of doxorubicin and related compounds in aqueous solution. *J Pharm Sci* 73:766–770.
- Miroux B, Walker JE (1996) Over-production of proteins in *Escherichia coli*: Mutant hosts that allow synthesis of some membrane proteins and globular proteins at high levels. *J Mol Biol* 260:289–298.
- Pos KM, Diederichs K (2002) Purification, crystallization and preliminary diffraction studies of AcrB, an inner-membrane multi-drug efflux protein. *Acta Crystallogr Biol Crystallogr* D58(Pt 10 Pt 2):1865–1867.
- Sambrook J, Fritsch EF, Maniatis T (1989) *Molecular Cloning: A Laboratory Manual* (Cold Spring Harbor Lab Press, Cold Spring Harbor, NY).
- Adler J, Lewinson O, Bibi E (2004) Role of a conserved membrane-embedded acidic residue in the multidrug transporter MdfA. *Biochemistry* 43:518–525.
- Kabsch W (2010) Integration, scaling, space-group assignment and post-refinement. *Acta Crystallogr D Biol Crystallogr* 66:133–144.
- Vagin AA, Teplyakov A (1997) MOLREP: An automated program for molecular replacement. *J Appl Cryst* 30:1022–1025.
- Storoni LC, McCoy AJ, Read RJ (2004) Likelihood-enhanced fast rotation functions. *Acta Crystallogr D Biol Crystallogr* 60:432–438.
- Adams PD, et al. (2010) PHENIX: A comprehensive Python-based system for macromolecular structure solution. *Acta Crystallogr D Biol Crystallogr* 66:213–221.
- Emsley P, Cowtan K (2004) Coot: Model-building tools for molecular graphics. *Acta Crystallogr Bio Crystallogr* 60(Pt 12 Pt 1):2126–2132.
- Krissinel E, Henrick K (2004) Secondary-structure matching (SSM), a new tool for fast protein structure alignment in three dimensions. *Acta Crystallogr D Biol Crystallogr* 60 (Pt 12 Pt 1):2256–2268.